ARL

US Army Research Laboratory

Study of the Bistatic Radar Cross Section of a 155-mm Artillery Round

by Christopher Kenyon and Traian Dogaru

NOTICES

Disclaimers

The findings in this report are not to be construed as an official Department of the Army position unless so designated by other authorized documents.

Citation of manufacturer's or trade names does not constitute an official endorsement or approval of the use thereof.

Destroy this report when it is no longer needed. Do not return it to the originator.

ARL

US Army Research Laboratory

Study of the Bistatic Radar Cross Section of a 155-mm Artillery Round

by Christopher Kenyon and Traian Dogaru
Sensors and Electron Devices Directorate, ARL

REPORT DOCUMENTATION PAGE

Form Approved
OMB No. 0704-0188

Public reporting burden for this collection of information is estimated to average 1 hour per response, including the time for reviewing instructions, searching existing data sources, gathering and maintaining the data needed, and completing and reviewing the collection information. Send comments regarding this burden estimate or any other aspect of this collection of information, including suggestions for reducing the burden, to Department of Defense, Washington Headquarters Services, Directorate for Information Operations and Reports (0704-0188), 1215 Jefferson Davis Highway, Suite 1204, Arlington, VA 22202-4302. Respondents should be aware that notwithstanding any other provision of law, no person shall be subject to any penalty for failing to comply with a collection of information if it does not display a currently valid OMB control number.
PLEASE DO NOT RETURN YOUR FORM TO THE ABOVE ADDRESS.

1. REPORT DATE *(DD-MM-YYYY)*	2. REPORT TYPE	3. DATES COVERED (From - To)
June 2017	Technical Report	Sep 2016–Apr 2017

4. TITLE AND SUBTITLE	5a. CONTRACT NUMBER
Study of the Bistatic Radar Cross Section of a 155-mm Artillery Round	
	5b. GRANT NUMBER
	5c. PROGRAM ELEMENT NUMBER
6. AUTHOR(S)	5d. PROJECT NUMBER
Christopher Kenyon and Traian Dogaru	
	5e. TASK NUMBER
	5f. WORK UNIT NUMBER

7. PERFORMING ORGANIZATION NAME(S) AND ADDRESS(ES)	8. PERFORMING ORGANIZATION REPORT NUMBER
US Army Research Laboratory ATTN: RDRL-SER-U 2800 Power Mill Road Adelphi, MD 20783-1138	ARL-TR-8045

9. SPONSORING/MONITORING AGENCY NAME(S) AND ADDRESS(ES)	10. SPONSOR/MONITOR'S ACRONYM(S)
	11. SPONSOR/MONITOR'S REPORT NUMBER(S)

12. DISTRIBUTION/AVAILABILITY STATEMENT

Approved for public release; distribution unlimited.

13. SUPPLEMENTARY NOTES

14. ABSTRACT

This report investigates the bistatic radar signature of a 155-mm artillery round in 4 radar frequency bands, L, S, C, and X, using computer models. The radar cross section (RCS) calculations are performed by 2 different methods, implemented by the FEKO and AFDTD electromagnetic simulation software packages, over all the possible aspect angles. The solutions obtained by the 2 methods are compared for accuracy validation, showing excellent agreement between the 2. We also include a discussion of the RCS results, which underscores the complexity of bistatic radar scattering phenomenology. Particular emphasis is given to the forward and specular scattering directions, which display much larger target signatures than other geometries, including that of a monostatic radar system.

15. SUBJECT TERMS

computational electromagnetics, radar signature, bistatic radar, radar cross section, RCS, EM

16. SECURITY CLASSIFICATION OF:			17. LIMITATION OF ABSTRACT	18. NUMBER OF PAGES	19a. NAME OF RESPONSIBLE PERSON
a. REPORT	b. ABSTRACT	c. THIS PAGE			Traian Dogaru
			UU	28	19b. TELEPHONE NUMBER (Include area code)
Unclassified	Unclassified	Unclassified			(301) 394-1482

Standard Form 298 (Rev. 8/98)
Prescribed by ANSI Std. Z39.18

Contents

List of Figures

INTENTIONALLY LEFT BLANK.

1. Introduction

The US Army has been developing radar technology for the detection and tracking of artillery rounds grouped under the generic category of rockets, artillery, and mortar. The electromagnetic (EM) modeling team at the US Army Research Laboratory (ARL) is contributing to these efforts by undertaking a systematic study of the radar signature of these targets, based on computer models. Our findings have already been published in a series of technical reports.[1–3] In those studies, we analyzed the radar cross section (RCS) of several types of projectiles for sensing scenarios involving monostatic radar. In this new report, we investigate the scattering signature obtained in bistatic radar configurations.

There has been little material published in the open literature on the subject of bistatic radar. Besides Willis' book,[4] which represents a good, systematic introduction to the topic, several other texts include chapters or research articles on bistatic radar.[5,6] However, the subject of bistatic RCSs is very briefly treated in all of these books. As discussed by many authors, one of the potential advantages of using bistatic radar is that, for many targets, the RCS in the forward and specular directions can be much larger (by orders of magnitude) than in the backscatter direction (where a monostatic radar operates). This can have a significant effect in improving the radar detection performance. However, these bistatic radar configurations also present serious drawbacks regarding the radar measurement of various target parameters[4]; therefore, the bistatic radar overall performance analysis always involves some engineering tradeoffs.

Our goal in this study is to understand the phenomenology of the bistatic radar scattering from a 155-mm artillery round, while limiting our analysis to scenarios amenable to an open-source publication. Specifically, we use computer simulations to calculate the bistatic RCS of this target placed in a fixed, upright position, without any reference to specific radar implementations or operational scenarios. As with our previous similar investigations, we use the AFDTD simulation software[7] to evaluate the RCS for all possible bistatic radar geometrical configurations, as well as 4 different radar frequency bands. As a preliminary step, we perform a validation of the AFDTD results with the commercial FEKO EM simulation software.[8]

This report is organized as follows. In Section 2, we present the target under investigation and the numerical methods used in computing the radar signature; additionally, we explain the geometry, notations, and terminology employed throughout the rest of the study. Section 3 compares the accuracy of the 2 EM modeling software packages used in this work. In Section 4, we discuss the relevant

phenomenology related to the bistatic RCS of the target as a function of aspect and frequency. We end with conclusions in Section 5.

2.   Description of the Target, Computational Methods, and Terminology

The radar target under investigation in this report, a 155-mm artillery round, is shown in Fig. 1. This is the same target used in our previous work on monostatic radar signatures.[1] As in that work, the projectile shell material is modeled as a perfect electric conductor. The closest simple geometrical shape, whose signature is discussed in some bistatic radar references,[4,9] is a circular cylinder of a diameter much smaller than its length. Knott includes a discussion of the physical optics solution to the radar scattering from a cylindrical target; however, that solution has a limited range of validity is terms of aspect angles and frequencies. Willis presents bistatic scattering patterns for a cylinder based on method of moments calculations, which were validated by measurements. The results in these references constitute a useful baseline for our investigation. Nevertheless, we expect the bistatic RSC of a 155-mm round to differ from that of a cylinder at certain aspect angles, given the nose taper characteristic of the former.
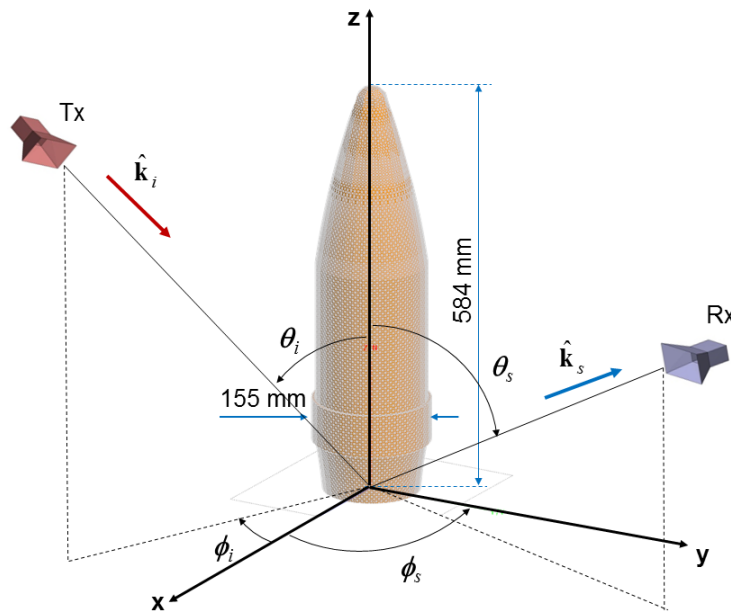

Fig. 1   Representation of the computational mesh of the 155-mm artillery round considered in this study, together with the Cartesian coordinate system and the incidence and scattering angles relevant to the bistatic radar geometry

Two different EM modeling programs were used in this study: FEKO and AFDTD. FEKO is a commercial software package that includes several methods of solving

general EM wave propagation problems, including radar scattering. In this work, we used the surface integral equation (SIE) solver (also known as the method of moments) for the RCS calculation of the targets of interest. AFDTD is an EM modeling software package developed in-house at ARL specifically for radar signature simulation. It is based on the finite-difference, time-domain (FDTD) method[10] and has been employed and validated in many radar system modeling applications of interest to the Army.

The AFDTD code was parallelized and designed to run on high-performance computing platforms at the Defense Supercomputing Resource Centers (DSRCs). For this investigation, the following platforms have been used: Excalibur (Cray XC40) at the ARL DSRC,[11] and Lightning (Cray XC30) at the US Air Force Research Laboratory DSRC.[12] The typical number of cores used in each simulation was 4. FEKO was run on desktop PCs under the Windows operating system, using a maximum of 4 cores at a time and with a memory limit of 96 GB. A more extensive comparison between the capabilities, limitations, and efficiency of the 2 software packages, relevant to the simulations presented in this study, was discussed in a previous report[1] and is not repeated here. An additional feature of both codes, which makes them particularly efficient to the current analysis, is the fact that they are capable of computing the bistatic RCS over the entire range of scattering angles, in one run. Nonetheless, the main purpose of employing 2 different simulation methods in this report is to validate the accuracy of their bistatic radar scattering calculations (this is performed in Section 3).

In reference to Fig. 1, we need to be specific about the way we define the incidence and scattering angles. Note that this report designates these angles in a manner consistent with the EM modeling codes (both AFDTD and FEKO), which may be different from other authors' notation. Thus, the target is placed at the origin of the Cartesian coordinate system and the radar transmitter (Tx) and receiver (Rx) are both placed in the far-field region. The pair of incidence angles (ϕ_i, θ_i) represents the direction of the Tx location, while the pair of scattering angles (ϕ_s, θ_s) represents the direction of the Rx location, both starting from the origin (see Fig. 1). The propagation directions of the incident and scattered plane waves are given by the following unit vectors:

$$\hat{\mathbf{k}}_i = \begin{bmatrix} -\cos\phi_i \sin\theta_i \\ -\sin\phi_i \sin\theta_i \\ -\cos\theta_i \end{bmatrix} \qquad \hat{\mathbf{k}}_s = \begin{bmatrix} \cos\phi_s \sin\theta_s \\ \sin\phi_s \sin\theta_s \\ \cos\theta_s \end{bmatrix} \qquad (1)$$

Notice that the ϕ angles are allowed to vary around the clock (from 0° to 360°), whereas the θ angles are limited to the interval between 0° and 180°. The backscattering configuration (encountered in monostatic radar) involves the following relations: $\phi_s = \phi_i$ and $\theta_s = \theta_i$. Other important bistatic scattering configurations are forward scattering, when $\phi_s - \phi_i = 180°$ and $\theta_i + \theta_s = 180°$; and specular scattering, when $\phi_s = \phi_i$ and $\theta_i + \theta_s = 180°$ (note that the term "specular" is used here in reference to the vertical axis of the target). These configurations are illustrated in Fig. 2. When the Tx, the target, and the Rx are all in the same vertical plane (meaning $\phi_s - \phi_i = 0°$ or 180°), we talk about "in-plane" scattering (Fig. 3a). When $\phi_s - \phi_i$ takes any other values, the scattering geometry is called "out-of-plane" (Fig. 3b).

(a)   (b)   (c)
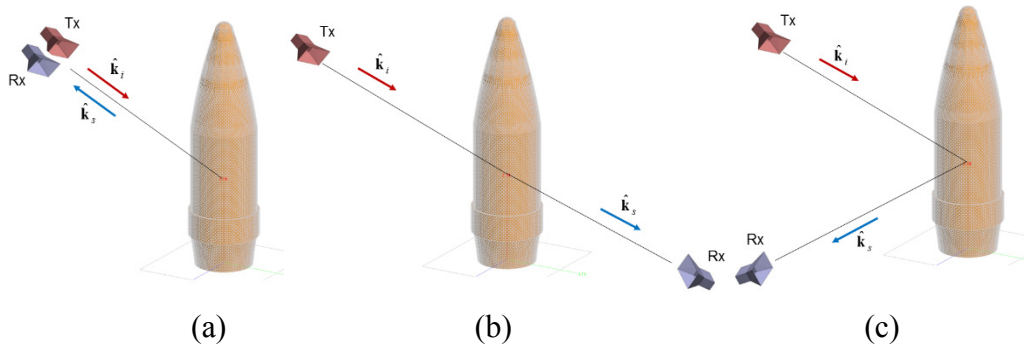
Fig. 2   Schematic diagram of 3 radar scattering geometries, showing the a) backscattering configuration, b) forward scattering configuration, and c) specular scattering configuration

(a)   (b)
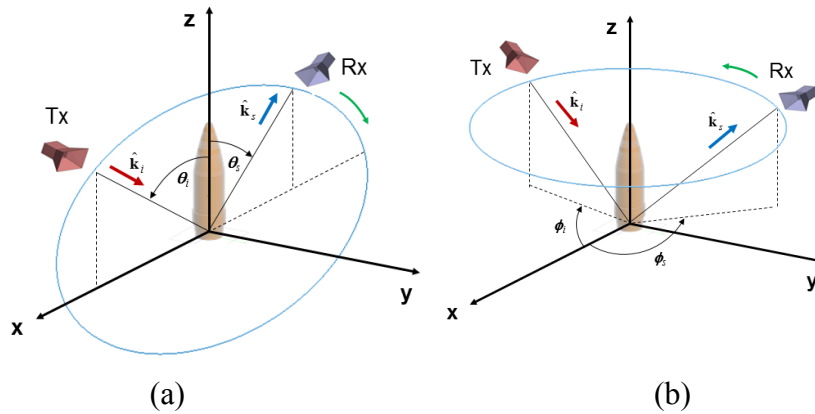
Fig. 3   Schematic diagram of 2 angle sweeping configurations, showing a) in-plane scattering and b) out-of-plane scattering

The simulation space for a bistatic radar signature is much larger than in the case of monostatic radar. Thus, when we characterize the RCS in the most general case, we have to deal with 5 variables: the 4 angles $\phi_i, \phi_s, \theta_i, \theta_s$ and frequency. In our

case, we take advantage of the target symmetry to reduce the dimensionality of the simulations and results. Thus, given the rotational symmetry with respect to the z axis, we can fix the angle ϕ_i (by taking $\phi_i = 0°$) and vary the angle ϕ_s from 0° to 180°, in 6° increments. Nevertheless, both θ angles must be swept from 0° to 180° in the simulations—we use 1° increments in this process. Another interesting result allowing us to reduce the simulation space is that the θ_i and θ_s angles are interchangeable (meaning that if we swap the values of θ_i and θ_s we obtain the same RCS)—this is a consequence of the reciprocity theorem in EM.[9]

In terms of frequencies, we perform the calculations at 1.3 GHz (corresponding to the L band), 2.4 GHz (to the S band), 5.6 GHz (to the C band), and 9.5 GHz (to the X band). For each band, the RCS results are averaged over a 200-MHz subband centered at the frequencies previously mentioned (similar to our previous work).[1,2] Additionally, we consider all polarization combinations: vertical-vertical (V-V), horizontal-horizontal (H-H), horizontal-vertical (H-V), and vertical-horizontal (V-H). The simulation results are typically presented as the variation of RCS in decibel square meters versus one angle.

3.   Comparison of FEKO and AFDTD Bistatic RCS Predictions

In this section, we present the results of the AFDTD and FEKO simulations for the target introduced in Section 2. A discussion of these results is included in Section 4. In Figs. 4 and 5, we compare the in-plane bistatic RCS obtained by the 2 methods, for V-V and H-H polarizations, in the S and X bands, respectively. For these simulations, we consider several incidence directions (θ_i = 30°, 60°, 90°, 120°, 150°) and let the θ_s angle vary around the clock. Notice that in Figs. 4 and 5, when the θ_s angle is positive (between 0° and 180°), we take ϕ_s = 180°, whereas when θ_s is negative (between 0° and –180°), we take ϕ_s = 0°. The arrows in these figures help the reader locate the backscatter, specular, and forward scattering directions in each case.

In Figs. 6–9, we compare the out-of-plane bistatic RCS obtained by the 2 methods. This time, we show only the S-band results, but consider all 4 polarization combinations (V-V, V-H, H-V, and H-H). In these figures, the pick the same 5 incidence directions (θ_i = 30°, 60°, 90°, 120°, 150°), as well as 5 different values of θ_s (θ_s = 30°, 60°, 90°, 120°, 150°), and let the angle ϕ_s vary from 0° and 180° (by symmetry, the other half of the circular range for ϕ_s would yield the same results). In Figs. 6–9, all the line plots were obtained with AFDTD, while the marker plots were obtained with FEKO. The specific values for θ_s in each plot of a graph are color-coded, as explained in the captions. In all cases, the match between the AFDTD and FEKO results is remarkably good.

(a)

(b)

(c)

(d)

(e)
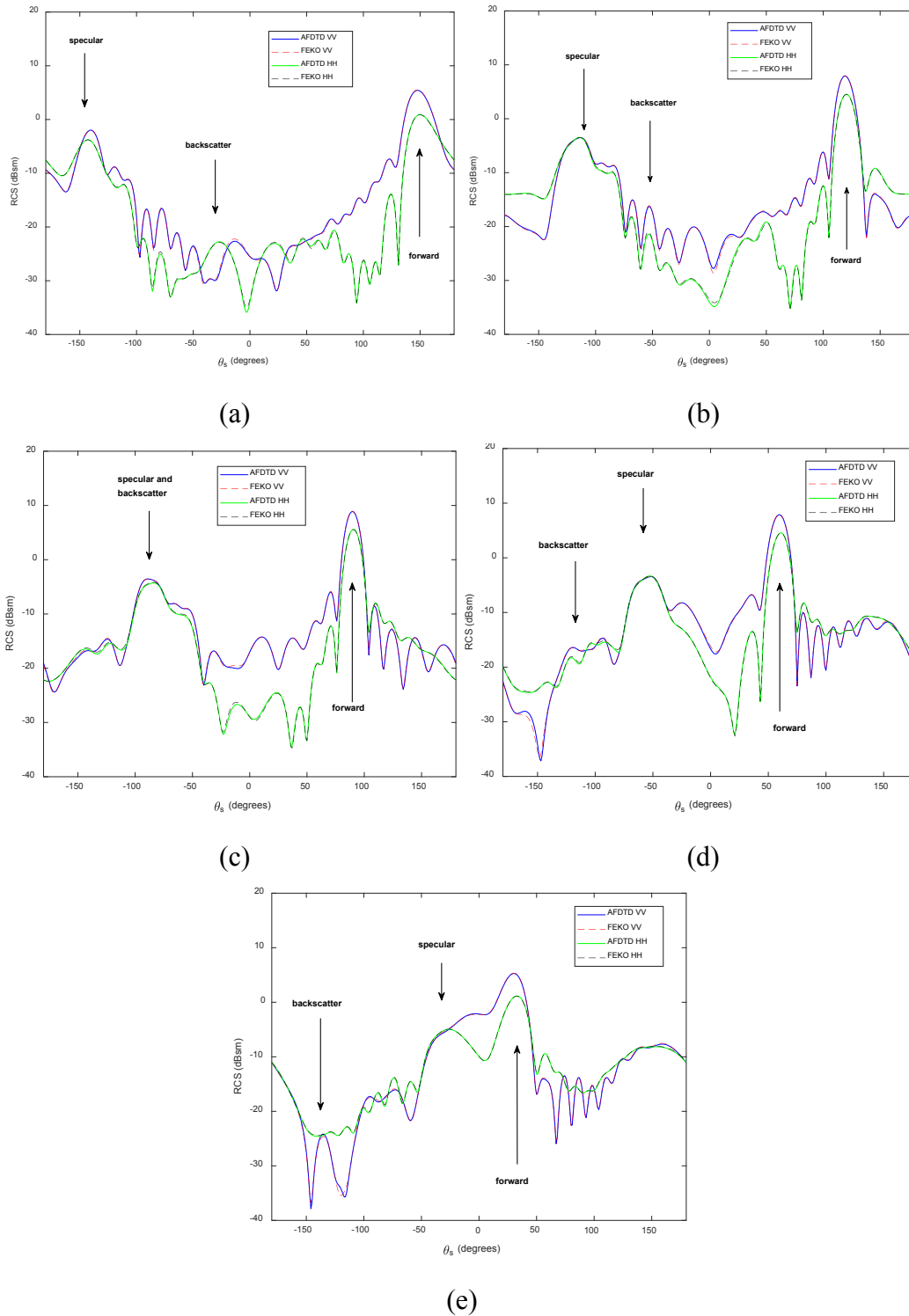
Fig. 4   In-plane bistatic RCS of a 155-mm round in the S band computed by AFDTD and FEKO for a) $\theta_i = 30°$, b) $\theta_i = 60°$, c) $\theta_i = 90°$, d) $\theta_i = 120°$, and e) $\theta_i = 150°$. In most cases, the lines obtained by the 2 methods are on top of one another.
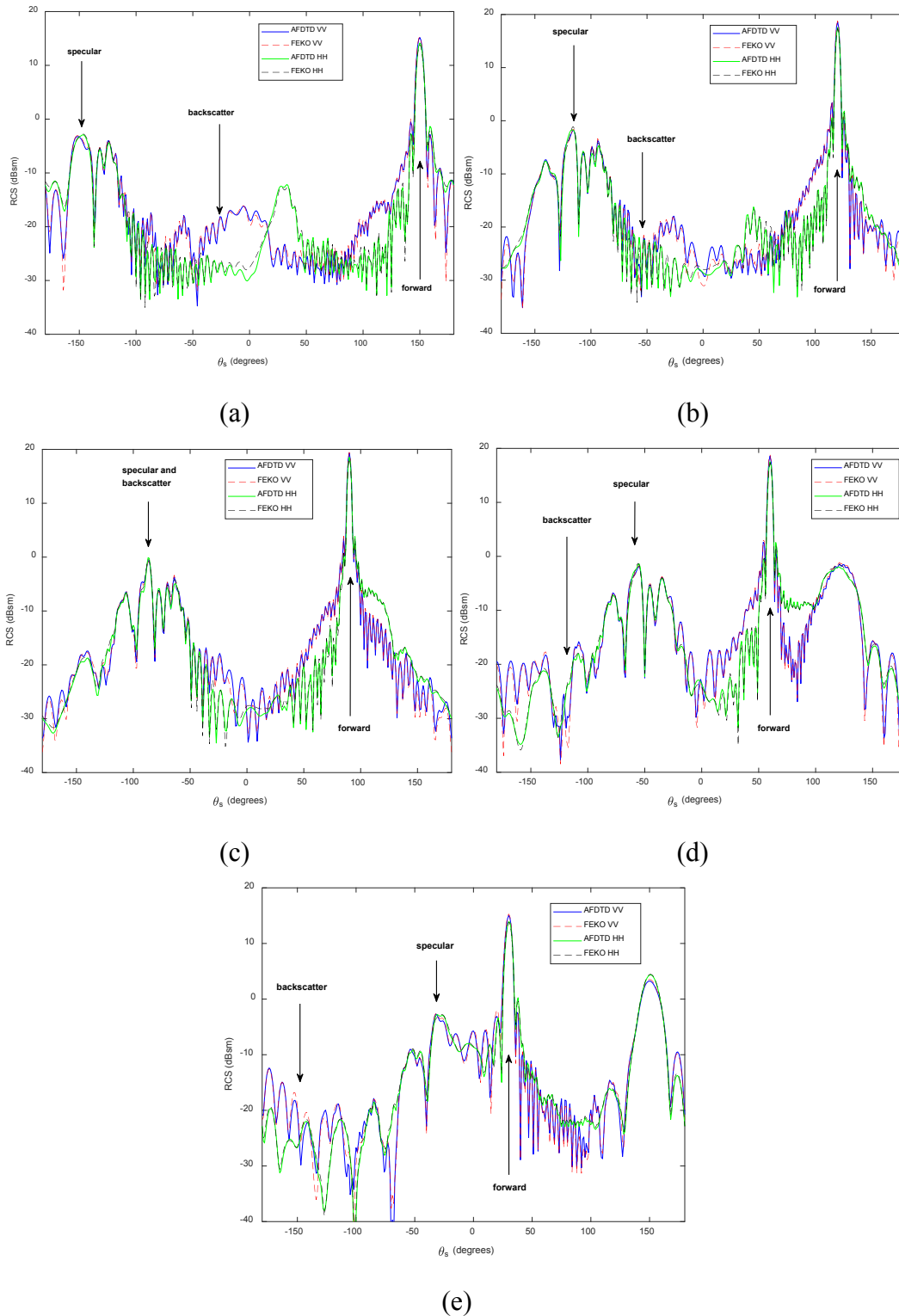
Fig. 5   In-plane bistatic RCS of a 155-mm round in the X band computed by AFDTD and FEKO for a) θ_i = 30°, b) θ_i = 60°, c) θ_i = 90°, d) θ_i = 120°, and e) θ_i = 150°. In most cases, the lines obtained by the 2 methods are on top of one another.

7

Fig. 6   Out-of-plane bistatic RCS of a 155-mm round in the S band computed by AFDTD and FEKO for V-V polarization and a) $\theta_i = 30°$, b) $\theta_i = 60°$, c) $\theta_i = 90°$, d) $\theta_i = 120°$, and e) $\theta_i = 150°$. The line plots were obtained by AFDTD, while the marker plots were obtained by FEKO. The plots are color-coded as follows: blue $\theta_s = 30°$, red $\theta_s = 60°$, green $\theta_s = 90°$, black $\theta_s = 120°$, and cyan $\theta_s = 150°$.

(a)

(b)

(c)

(d)

(e)

Fig. 7   Out-of-plane bistatic RCS of a 155-mm round in the S band computed by AFDTD and FEKO for H-H polarization and a) $\theta_i = 30°$, **b)** $\theta_i = 60°$, **c)** $\theta_i = 90°$, **d)** $\theta_i = 120°$, **and e)** $\theta_i = 150°$. **The line plots were obtained by AFDTD, while the marker plots were obtained by FEKO. The plots are color-coded as follows: blue** $\theta_s = 30°$, **red** $\theta_s = 60°$, **green** $\theta_s = 90°$, **black** $\theta_s = 120°$, **and cyan** $\theta_s = 150°$.

9
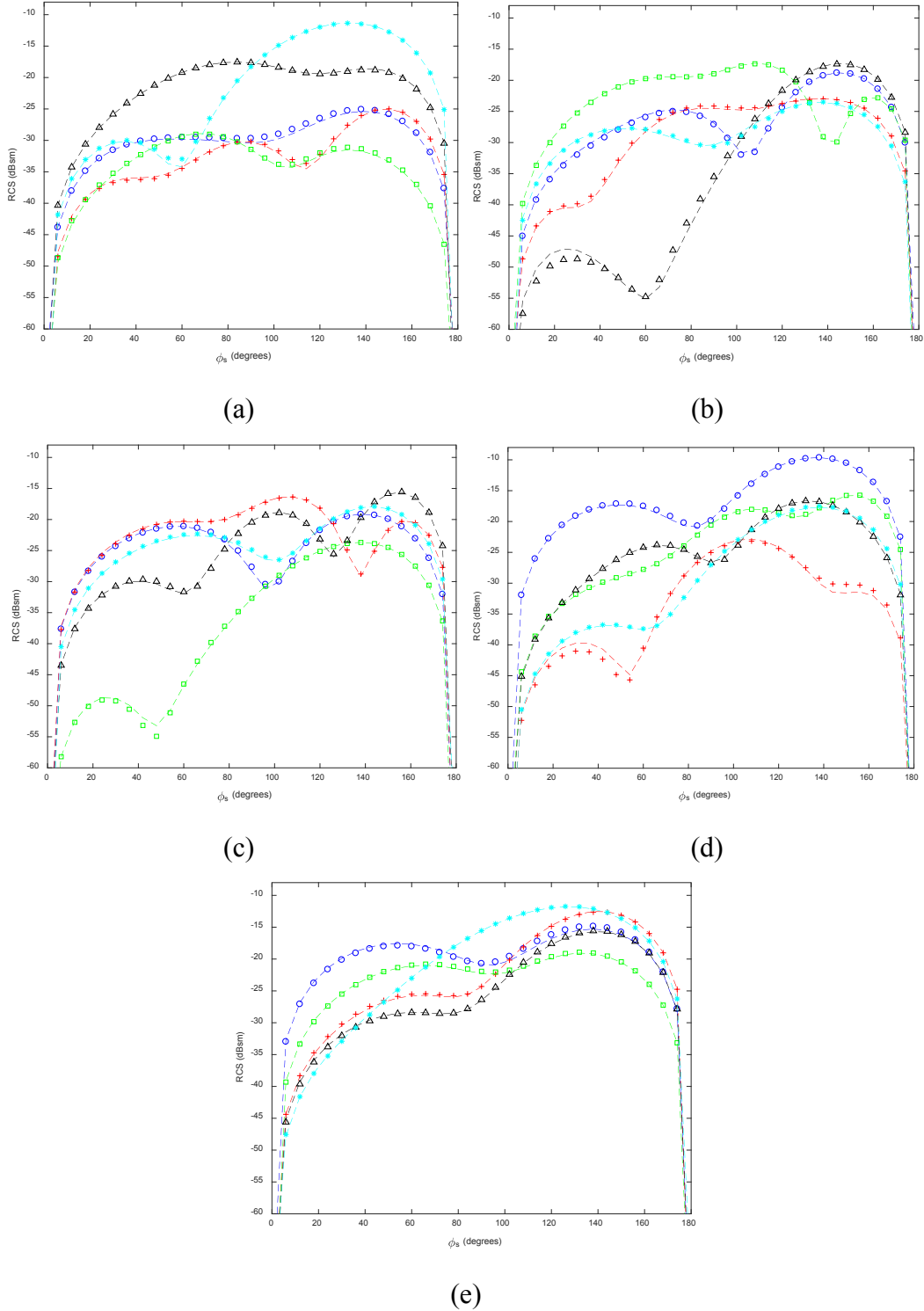
Fig. 8   **Out-of-plane bistatic RCS of a 155-mm round in the S band computed by AFDTD and FEKO for H-V polarization and a)** $\theta_i = 30°$, **b)** $\theta_i = 60°$, **c)** $\theta_i = 90°$, **d)** $\theta_i = 120°$, **and e)** $\theta_i = 150°$. **The line plots were obtained by AFDTD, while the marker plots were obtained by FEKO. The plots are color-coded as follows: blue** $\theta_s = 30°$, **red** $\theta_s = 60°$, **green** $\theta_s = 90°$, **black** $\theta_s = 120°$, **and cyan** $\theta_s = 150°$.
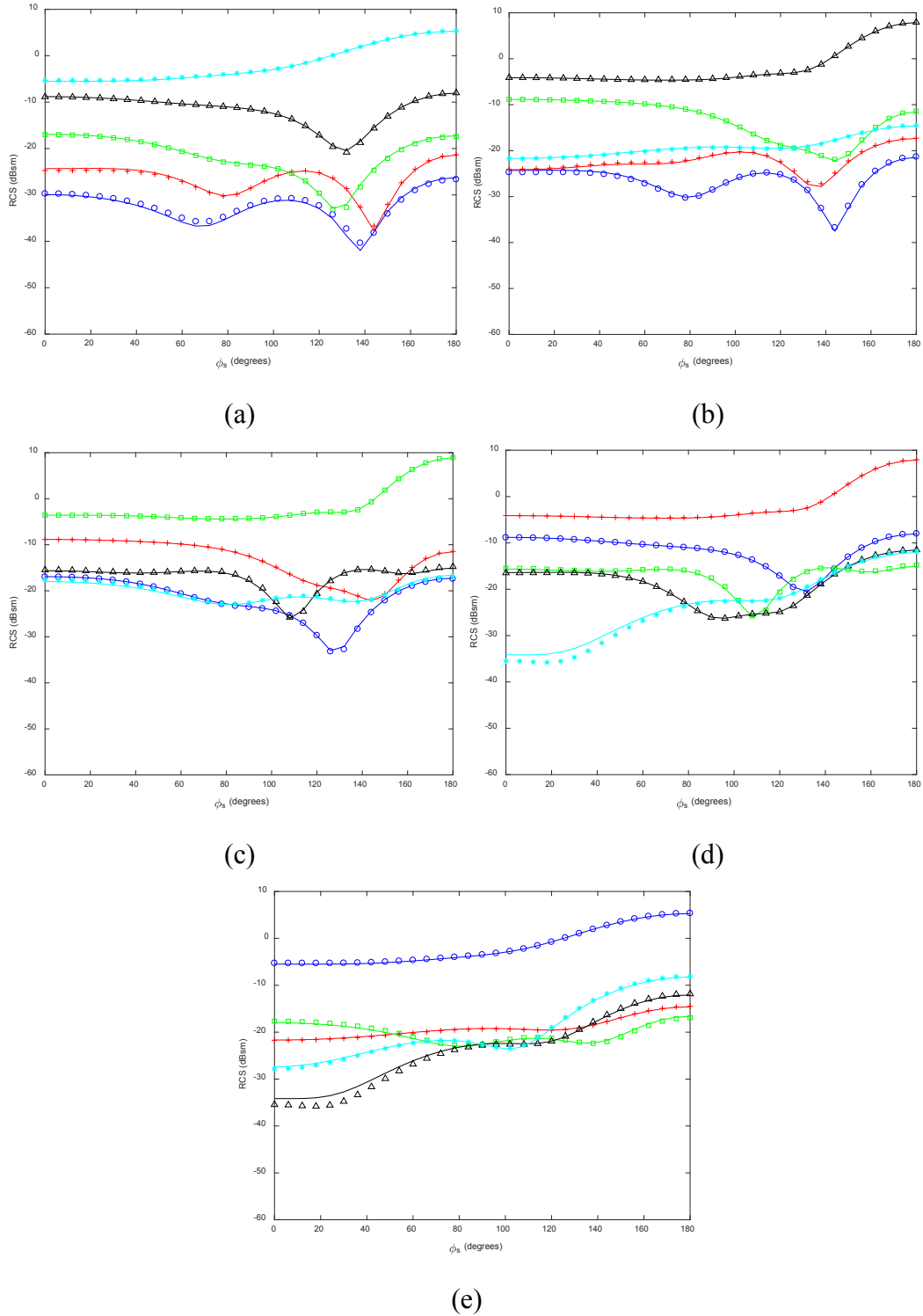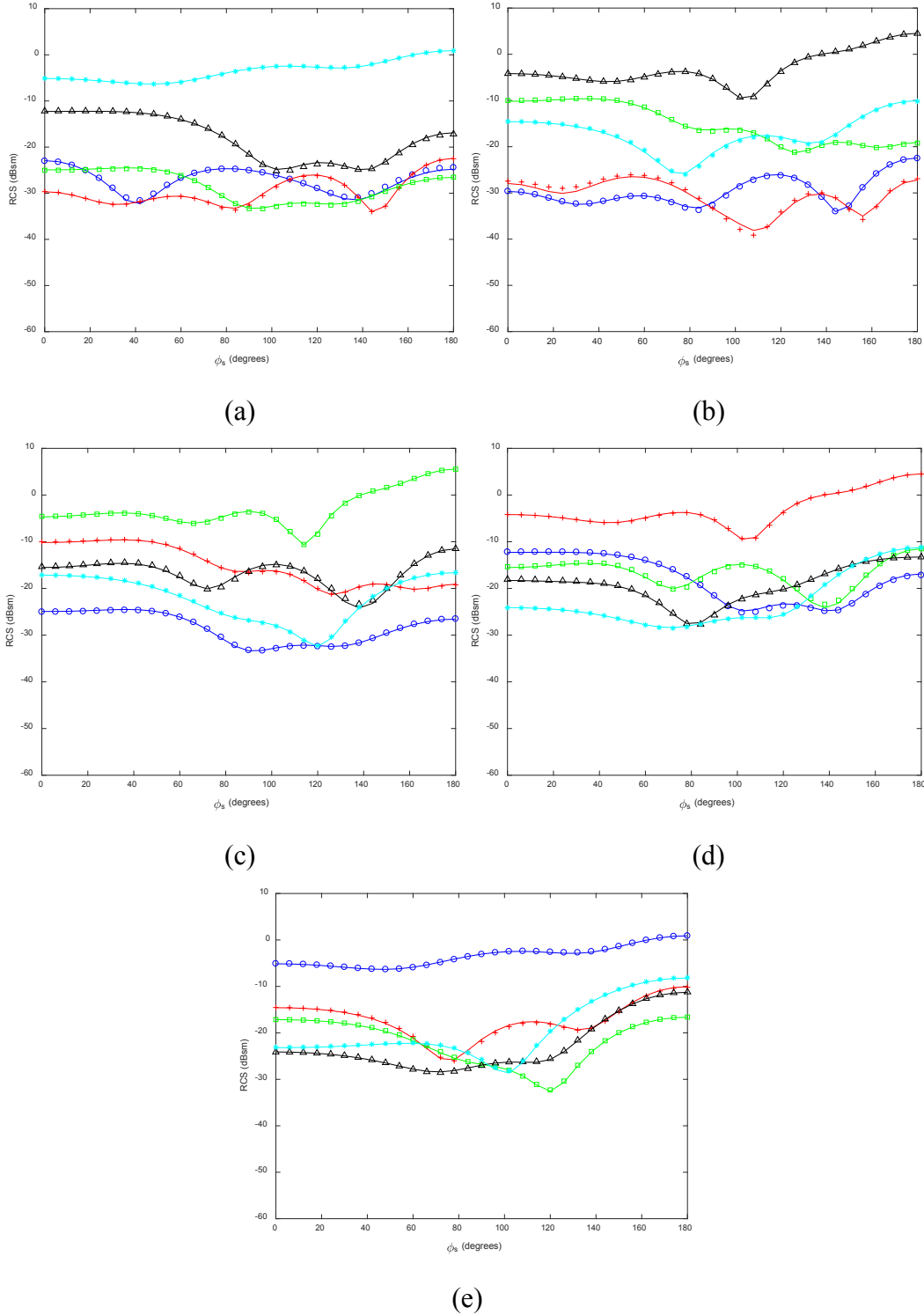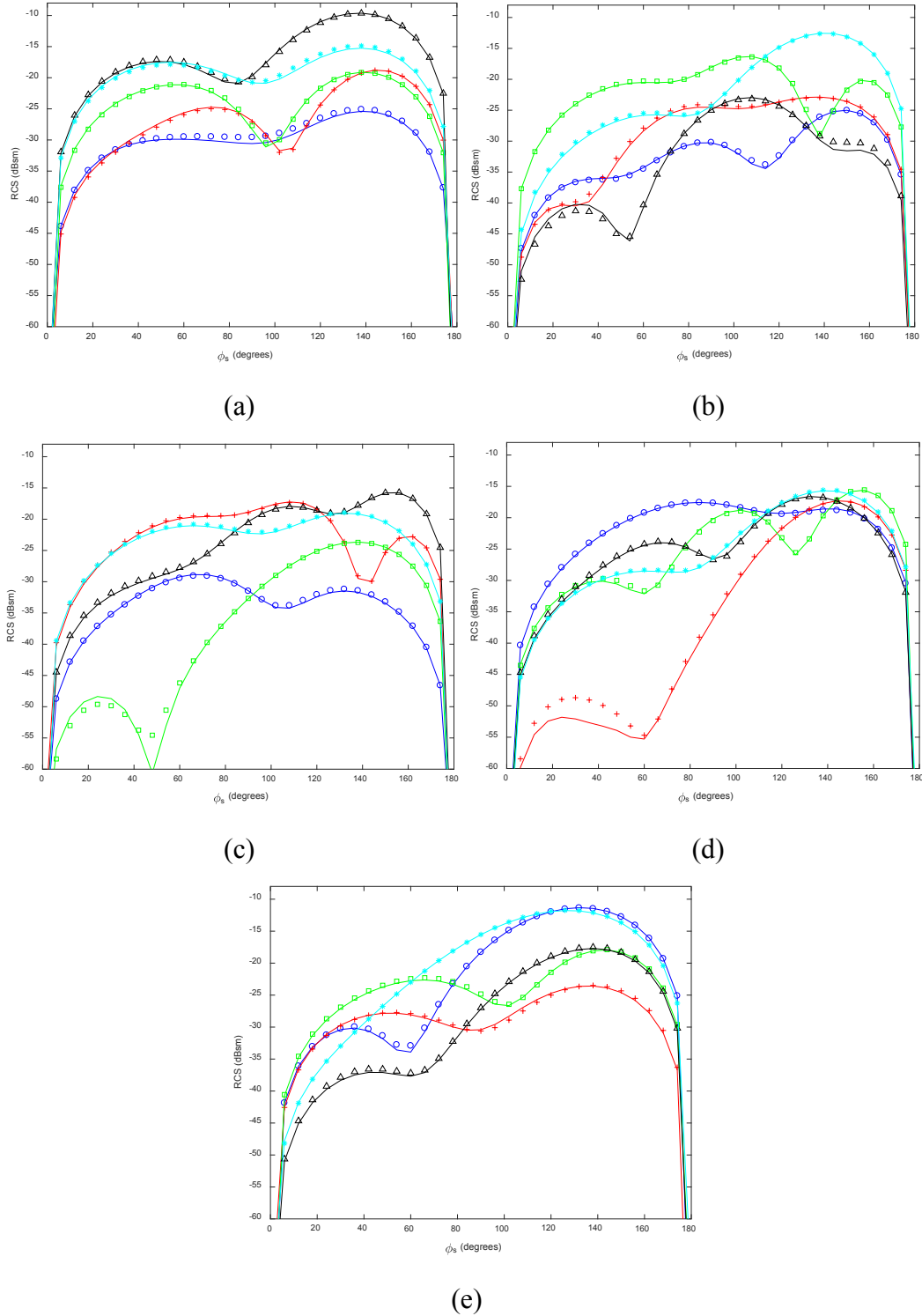
Fig. 9   Out-of-plane bistatic RCS of a 155-mm round in the S band computed by AFDTD and FEKO for V-H polarization and a) $\theta_i = 30°$, b) $\theta_i = 60°$, c) $\theta_i = 90°$, d) $\theta_i = 120°$, and e) $\theta_i = 150°$. The line plots were obtained by AFDTD, while the marker plots were obtained by FEKO. The plots are color-coded as follows: blue $\theta_s = 30°$, red $\theta_s = 60°$, green $\theta_s = 90°$, black $\theta_s = 120°$, and cyan $\theta_s = 150°$.

11

4.   Discussion of the Bistatic RCS of a 155-mm Round

In this section, we discuss some of the bistatic signature results from Section 3 and make a comparison of the bistatic RCS over the 4 frequency bands mentioned in Section 2. Although the simulations were run over the entire angular ranges mentioned in Section 2, we must limit the presentation of results to a relatively small number of scenarios. In previous work,[1,2] the comparison among frequency bands was performed by computing monostatic RCS averages over the scattering elevation angle. We attempted a similar procedure for the bistatic RCS: for instance, one could fix the θ_i and θ_s angles, and compute averages over $\phi_s - \phi_i$. However, we found out that such averages are clearly dominated by 2 angular configurations (corresponding to forward and specular scattering), where the RCS is typically at least an order of magnitude larger than in other directions. Consequently, we think that the RCS averages over certain angular ranges are less meaningful for our investigation; instead, we decided to simply compare the scattering strengths in the forward and specular directions among the 4 frequency bands.

The bistatic RCS results for in-plane scattering (Figs. 4 and 5) show, as expected, 2 peaks, in the forward and specular directions. Notice that the difference between these 2 peaks becomes larger as the incidence direction gets closer to normal to the target ($\theta_i = 90°$). For $\theta_i = 90°$, the forward scattering configuration reaches the absolute maximum in terms of RCS. For smaller θ_i (or incidence direction closer to the z axis), the peaks are not very pronounced: in that case, the target geometry as seen by the radar Tx departs the ideal long cylindrical shape and the contribution of the projectile's ends to the scattering response becomes more significant. The peaks in the forward and specular directions become narrower as the frequency is increased (compare the plots in the S and X bands), meaning that, at high frequency, the scattering is more directional.

More interesting are the RCS results for out-of-plane bistatic scattering. By analyzing the plots in Figs. 6–9, we concluded (again, as expected) that configurations for which $\theta_s + \theta_i = 180°$ (which contain both the forward and specular directions) display the largest RCS at any azimuth angle. However, when one tries to compare the RCS in the general "forward scattering hemisphere" (where $90° \leq \phi_s - \phi_i \leq 180°$) with that in the "backward scattering hemisphere" (where $0° \leq \phi_s - \phi_i \leq 90°$), the results are less clear-cut. Thus, for configurations where $\theta_s + \theta_i = 180°$, the RCS in the forward hemisphere is generally larger than that in the backward hemisphere. However, for $\theta_s + \theta_i \neq 180°$, there are

configurations where the opposite is true. Another striking result is the fact that, in the backward hemisphere, the bistatic RCS generally does not vary much with the azimuth angle ($\phi_s - \phi_i$), typically within a range of no more than 5 dB. This effect is more evident as the incidence gets closer to normal to the target ($\theta_i = 90°$).

So far, the discussion involved only the 2 co-polarized scattering configurations, V-V and H-H. The in-plane cross-polarization (i.e., V-H and H-V) bistatic signature is theoretically null due to the target symmetry—consequently, we did not display it graphically in this report. However, as shown in Figs. 6–9, the out-of-plane cross-polarization RCS can be quite significant—at some scattering angles, especially as ϕ_s approaches 90º, it exceeds the co-polarization RCS. This result is important for radar systems that measure fully polarimetric data and may open the door to interesting applications of polarimetric processing for bistatic radar. Another interesting fact is that the signatures are different between V-H and H-V polarizations for bistatic radar configurations. This is unlike for a monostatic radar, where the 2 cross-polarization combinations yield the same signature. This means that as far as polarization goes, the bistatic radar is an example where the reciprocity principle cannot be applied.

Finally, we compare the bistatic RCS in the forward and specular directions among the 4 frequency bands in Figs. 10 and 11, for V-V and H-H polarizations, respectively. The angle variable in the graphs in Figs. 10 and 11 is θ_i. For $\theta_i = 0°$ or 180°, the specular and forward scattering directions are identical. In the forward direction, the RCS always has a peak for normal incidence, when $\theta_i = 90°$; however, the specular RCS does not display the same variation with θ_i, but is relatively flat. Interestingly, a simple analytic formula gives an approximate value of a target RCS in the forward scattering direction[4]:

$$\sigma_F = 4\pi \frac{A^2}{\lambda^2} \sin^2 \theta_i \qquad (2)$$

where A is the target's shadow area (in our case, the cross-section area in a vertical plane going through its middle) and λ is the radar wavelength. This formula becomes more accurate as we approach the "optical" (or high-frequency) regime. To test its accuracy, we plotted it alongside the AFDTD-computed values in Figs. 10 and 11 (note: for the 155-mm round, we have $A = 0.0765$ m^2). By comparing the graphs, we conclude that the analytic prediction is fairly close to the exact (AFDTD) solution, except for incidence near nose-on or bottom-on orientations (within 30° from the z axis). The analytic formula's accuracy is better at high frequencies (X band) than at low frequencies (L band), and for H-H

polarization than for V-V polarization, but the errors never exceed 3 dB within the angular range already mentioned.
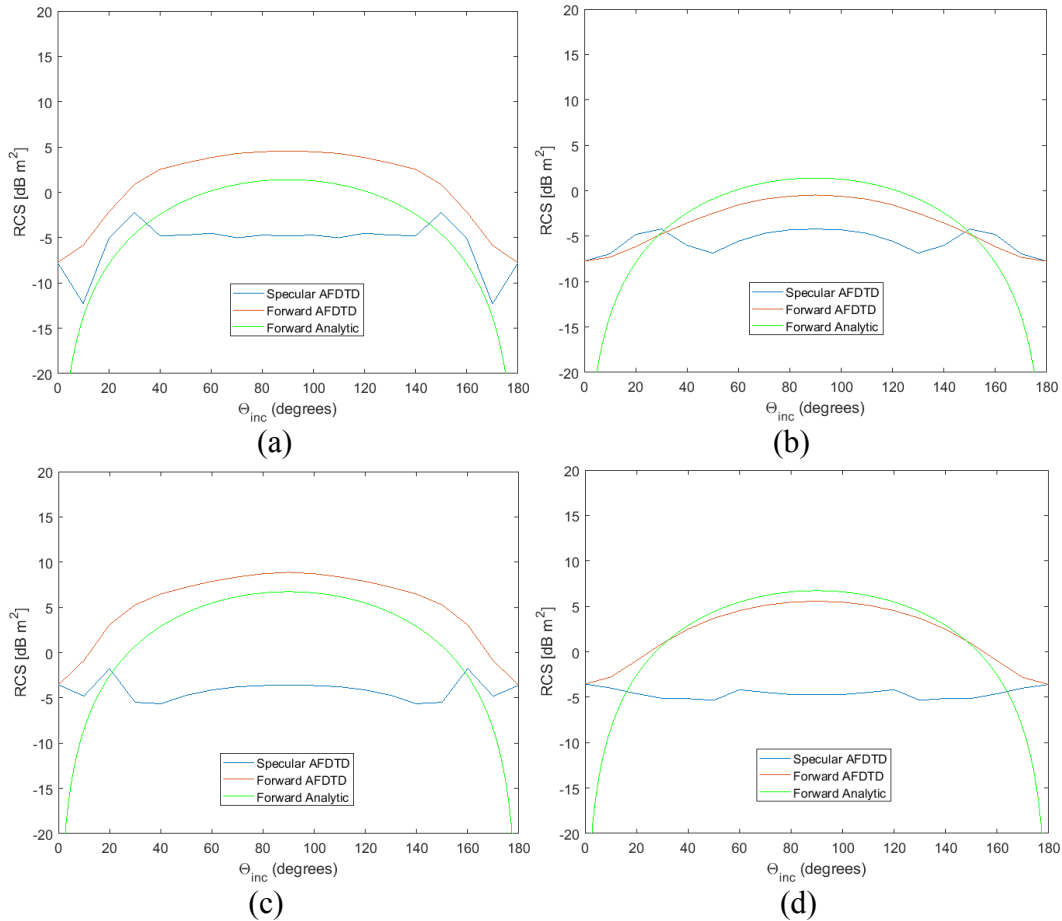

Fig. 10   Bistatic RCS of a 155-mm round in the forward and specular directions as a function of θ_i, showing a) L-band, V-V polarization; b) L-band, H-H polarization; c) S-band, V-V polarization; and d) S-band, H-H polarization
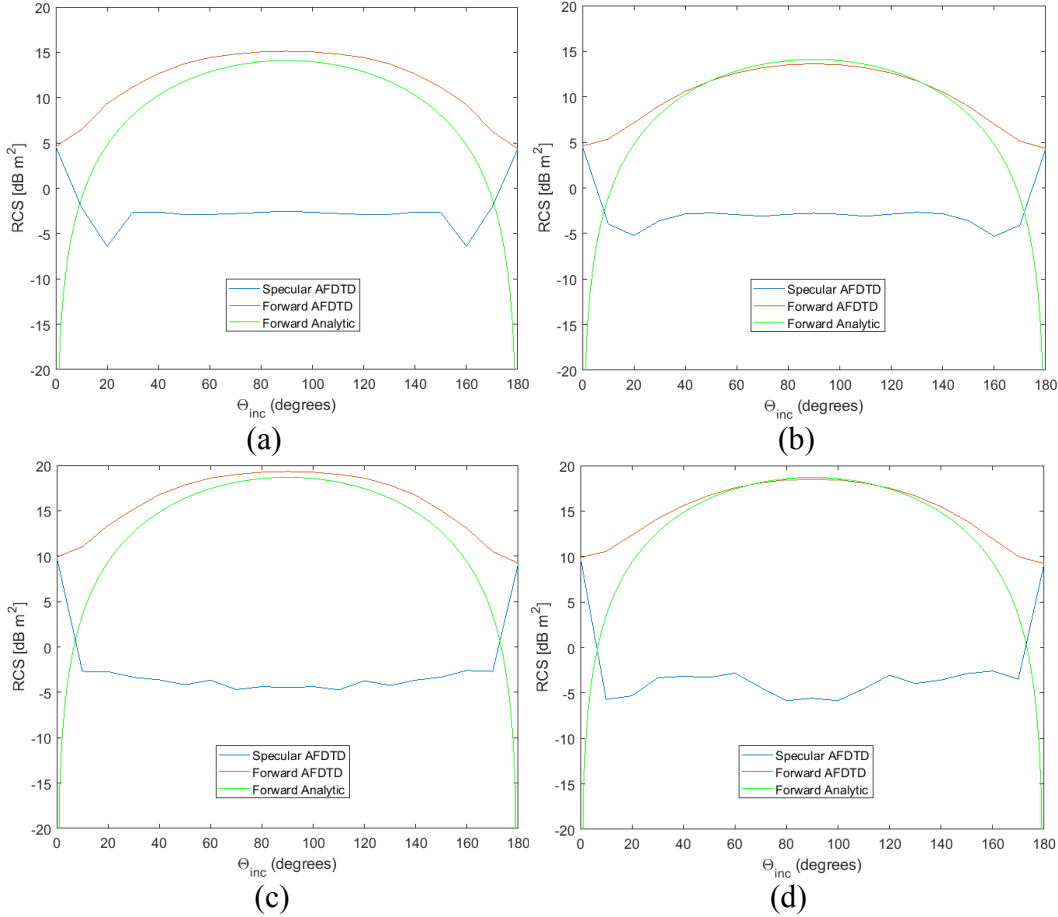
14

Fig. 11   Bistatic RCS of a 155-mm round in the forward and specular directions as a function of θ_i, showing a) C-band, V-V polarization; b) C-band, H-H polarization; c) X-band, V-V polarization; and d) X-band, H-H polarization

Regarding the frequency dependence, we notice larger forward and specular RCS values as the frequency increases. However, this does not necessarily mean that the RCS generally increases with frequency for all bistatic angle configurations. As previously discussed, the plots in Figs. 3–6 show that, as the frequency is increased, the forward and specular peaks become both narrower and larger in amplitude, leaving open the question whether the average bistatic RCS increases or decreases with frequency. For now, we can state that the answer to this question depends on the specific bistatic radar sensing scenario and geometry and will be the subject of a future study.

5.   Conclusions

This report performed an investigation of the RCS of 155-mm artillery round for bistatic radar configurations. As mentioned in the Introduction, very little information has been published in the open literature on the bistatic radar signature

of targets beyond some very basic shapes and approximate signature analysis methods. To obtain accurate bistatic RCS data on the target of interest, we employed exact EM modeling techniques, based on FDTD and the SIE methods. The software packages employed in our simulations were AFDTD and FEKO. The results obtained by the 2 codes are in very good agreement, as demonstrated in Section 3—this makes us confident to use them in future investigations related to this radar technology.

The bistatic RCS analysis in Section 4 suggests that the phenomenology of bistatic radar scattering is very complex and does not lend itself to simple generalizations, particularly for out-of-plane configurations. This is consistent with the findings of other authors; thus, Willis[4] warns against drawing simplified conclusions regarding the scattering signature of radar targets and clutter for bistatic geometries. Moreover, the target considered in this report has a particular shape displaying cylindrical symmetry; consequently, we need to clearly state that some results in Section 4 cannot be extended to the bistatic signature of other targets with different shape factors and symmetry characteristics.

Nevertheless, certain general conclusions can be drawn from our study regarding the bistatic RCS of the 155-mm round. Most importantly, there are 2 configurations, the forward and specular scattering, where the target signature is much larger (by at least an order of magnitude) than in any other geometries. Therefore, a bistatic radar system could potentially present a rather large advantage over a monostatic system in terms of radar signature. Nonetheless, multiple other issues related to the bistatic radar technology,[4] which are not discussed in this report, could either negate this advantage or make the bistatic radar implementation impractical. Follow-up investigations will attempt to further our understanding of these issues as they relate to practical radar detection problems of interest to the Army.

6. References

1. Kenyon C, Dogaru T. Numerical computation of the radar cross section of rockets and artillery rounds. Adelphi (MD): Army Research Laboratory (US); 2015 Sep. Report No.: ARL-TR-7468.

2. Kenyon C, Dogaru T. Numerical computation of the radar cross section of a 120-mm mortar. Adelphi (MD): Army Research Laboratory (US); 2015 Nov. Report No.: ARL-TN-0716.

3. Dogaru T, Kenyon C. Numeric computation of the radar cross section of in-flight Projectiles. Adelphi (MD): Army Research Laboratory (US); 2016 Nov. Report No.: ARL-TR-7895.

4. Willis N. Bistatic radar. Norwood (MA): Artech; 1991.

5. Skolnik M. Radar handbook. New York (NY): McGraw Hill; 2008.

6. Melvin W, Scheer J. Principles of modern radar – radar applications. Raleigh: SciTech Publishing; 2014.

7. Dogaru T. AFDTD user's manual. Adelphi (MD): Army Research Laboratory (US); 2010 Mar. Report No.: ARL-TR-5145.

8. FEKO EM Simulation Software Web page. Tory (MI): Altair Engineering; 2015. [accessed 2016 Oct]. http://www.feko.info.

9. Knott E, Shaeffer J, Tuley M. Radar cross section. Norwood (MA): Artech; 1993.

10. Taflove A, Hagness S. Computational electrodynamics: The finite-difference time-domain method. Norwood (MA): Artech; 2000.

11. ARL DSRC Web page. Aberdeen Proving Ground (MD): Army Research Laboratory (US); 2016 Oct 18 [accessed 2017 May]. http://www.arl.hpc.mil.

12. AFRL DSRC Web page. Wright Patterson Air Force Base (OH): Air Force Reearch Laboratory (US); 2015 Aug 5 [accessed 2017 May]. http://www.afrl.hpc.mil.

List of Symbols, Abbreviations, and Acronyms

ARL   US Army Research Laboratory

DSRC   Defense Supercomputing Resource Center

EM   electromagnetic

FDTD   finite difference, time domain

H-H   horizontal-horizontal

H-V   horizontal-vertical

PC   personal computer

RCS   radar cross section

Rx   receiver

SIE   surface integral equation

Tx   transmitter

V-H   vertical-horizontal

V-V   vertical-vertical

| 1 | DEFENSE TECH INFO CTR |
| (PDF) | ATTN DTIC OCA |

2	US ARMY RSRCH LAB
(PDF)	ATTN IMAL HRA MAIL & RECORDS MGMT
	ATTN RDRL CIO LL TECHL LIB

| 1 | GOVT PRNTG OFC |
| (PDF) | ATTN A MALHOTRA |

7	US ARMY RSRCH LAB
(PDF)	RDRL SER U
	A SULLIVAN
	C KENYON
	C LE
	D LIAO
	T DOGARU
	RDRL SER M
	A HEDDEN
	D WIKNER

INTENTIONALLY LEFT BLANK.